Measurement of the beta-nu correlation coefficient a(beta nu) in the beta decay of trapped He-6(+) ions

X. Fléchard, P. Velten, E. Liénard, A. Méry, D. Rodríguez, G. Ban, D. Dominique Durand, F. Mauger, O. Naviliat-Cuncic, J.C. Thomas

Measurement of the β-ν correlation coefficient $a_{\beta\nu}$ in the β decay of trapped $^6He^+$ ions

X. Fléchard[1], Ph. Velten[1], E. Liénard[1], A. Méry[2], D. Rodríguez[3], G. Ban[1], D. Durand[1], F. Mauger[1], O. Naviliat-Cuncic[1,4], and J.C. Thomas[5]

[1] LPC Caen, ENSICAEN, Université de Caen, CNRS/IN2P3-ENSI, Caen, France

[2] CIMAP, CEA/CNRS/ENSICAEN, Université de Caen, Caen, France

[3] Departamento de Física Atómica, Molecular y Nuclear, Universitad de Granada, 18071, Granada, Spain

[4] NSCL and Department of Physics and Astronomy, Michigan State University, East-Lansing, MI, USA

[5] GANIL, CEA/DSM-CNRS/IN2P3, Caen, France

Email : flechard@lpccaen.in2p3.fr

Abstract

We have measured the β–ν angular correlation in the β decay of $^6He^+$ ions using a transparent Paul trap. The $^6He^+$ ions, produced at GANIL, were first cooled and bunched before being injected in the LPCTrap setup. The angular correlation was inferred from the time of flight of recoil nuclei detected in coincidence with the β particles. The detection system gives access to the full β decay kinematics, providing means to check the data reliability and to reject a large fraction of background. We find $a_{\beta\nu} = -0.3335(73)_{stat}(75)_{syst}$, in agreement with the Standard Model prediction for a pure Gamow-Teller transition.

PACS numbers: 23.20.En, 23.40.Bw, 24.80.+y, 37.10.Rs, 37.10.Ty, 13.30.Ce

1. Introduction

The generalization of Fermi's original theory of β decay allows for five different Lorentz invariant contributions to the β decay Hamiltonian. These are the scalar (*S*), vector (*V*), tensor (*T*), axial-vector (*A*), and pseudoscalar (*P*) interactions. The *P* interaction can be neglected in the non-relativistic description of nucleons, but the respective coupling constants C_i and C_i' (i = *S*, *V*, *A*, *T*) had to be determined from experiments. The existence of both, C_i and C_i' couplings, is related to transformation properties under parity, with $|C_i| = |C_i'|$ corresponding to maximum parity violation. The *V* and *A* character of the weak interaction, postulated by Feynman and Gell-Man [1], was experimentally established 50 years ago [2]. Within the *V-A* theory embedded in the Standard Model (SM), *S* and *T*-type interactions are excluded. However, the experimental constraints on these couplings (in particular assuming right handed couplings in the scalar and tensor sector) remain strikingly loose. A global analysis of data from both neutron and nuclear β decay experiments [3] yielded $|C_S / C_V| < 0.07$ and $|C_T / C_A| < 0.08$ (95.5% C.L.), which still allows sizeable scalar and tensor contributions.

The precise measurement of the beta-neutrino angular correlation coefficient, $a_{\beta\nu}$, in nuclear β decay is a direct and sensitive tool to search for *S* and *T* exotic contributions. For allowed transitions and non oriented nuclei, the angular correlation coefficient $a_{\beta\nu}$ can be inferred from the distribution in the electron and neutrino directions and in the electron energy [4]

$$\omega(E_e,\Omega_e,\Omega_\nu)=\frac{F(\pm Z,E_e)}{(2\pi)^5}p_eE_e(E_0-E_e)^2\frac{1}{2}\xi\left(1+a_{\beta\nu}\frac{\vec{p}_e\cdot\vec{p}_\nu}{E_eE_\nu}+b\frac{m}{E_e}\right) \quad (1)$$

where $E_e, \vec{p}_e$ and Ω_e denote the total energy, momentum, and angular coordinates of the β particle and similarly for the neutrino. $F(\pm Z,E_e)$ is the Fermi function (± sign referring to β^- and β^+ decays), E_0 is the total energy available in the transition, and m is the electron rest mass. The common factor ξ, $a_{\beta\nu}$, and the Fierz interference term b are determined by the fundamental weak coupling constants C_i and C_i' ($i = S, V, A, T$), and by the Fermi (Gamow-Teller) nuclear matrix elements M_F (M_{GT}):

$$\xi=|M_F|^2(|C_S|^2+|C_V|^2+|C_S'|^2+|C_V'|^2)+|M_{GT}|^2(|C_T|^2+|C_A|^2+|C_T'|^2+|C_A'|^2) \quad (2)$$

$$\begin{aligned}a_{\beta\nu}\xi=&|M_F|^2\left[|C_V|^2+|C_V'|^2-|C_S|^2-|C_S'|^2\mp2\frac{\alpha Zm}{p_e}\mathrm{Im}(C_SC_V^*+C_S^{'}C_V^{'*})\right]\\&+\frac{|M_{GT}|^2}{3}\left[|C_T|^2+|C_T'|^2-|C_A|^2-|C_A'|^2\pm2\frac{\alpha Zm}{p_e}\mathrm{Im}(C_TC_A^*+C_T^{'}C_A^{'*})\right]\end{aligned} \quad (3)$$

and

$$b=\pm2\sqrt{1-\alpha^2Z^2}\,\mathrm{Re}\left[|M_F|^2(C_SC_V^*+C_S'C_V'^*)+|M_{GT}|^2(C_TC_A^*+C_T'C_A'^*)\right]\xi^{-1} \quad (4)$$

We note that the $a_{\beta\nu}$ coefficient depends on the C_S and C_S' couplings in a pure Fermi transition, and on the C_T and C_T' couplings in a pure Gamow-Teller transition. In the SM, assuming maximal parity violation and neglecting effects due to *CP* violation in the light quark sector, $C_i = C_i'$ and $\mathrm{Im}(C_i) = \mathrm{Im}(C_i') = 0$ for $i = V, A$ and $C_i = C_i' = 0$ for $i = S, T$. The beta-neutrino angular correlation $a_{\beta\nu}$ is then given by

$$a_{\beta\nu}=\frac{1-\rho^2/3}{1+\rho^2} \quad (5)$$

where ρ is the mixing ratio

$$\rho=\frac{C_AM_{GT}}{C_VM_F} \quad (6)$$

leading to $a_{\beta\nu}=1$ for a pure Fermi transition, and $a_{\beta\nu}=-1/3$ for a pure Gamow-Teller transition. Since neutrinos are too difficult to detect, the most sensitive observable for an angular correlation measurement is the energy of the recoiling daughter nucleus.

In the past two decades, several precise measurements of the β–ν angular correlation in pure Fermi transitions were performed by measuring the Doppler shift of gamma rays following the β decay of ^{18}Ne [5] or the kinematic shifts of protons in ^{32}Ar decay [6]. More recently, measurements used the confinement of ^{38}K^m radioactive atoms in a magneto-optical trap (MOT) [7]. In that experiment, the atomic sample was held nearly at rest in high vacuum. The β particles and recoil ions were detected in coincidence with minimal disturbance from the environment, and the recoil ions energy was inferred from their time of flight. This experiment yielded a relative precision of 0.46%. Vetter *et al*. [8] used a similar technique to measure $a_{\beta\nu}$ in the mixed transition of ^{21}Na which resulted in a relative precision at the level of 1%. All these measurements, mainly probing the existence of scalar currents, were found in agreement with the SM predictions.

For pure Gamow-Teller transitions, the last experiments were performed nearly fifty years ago in the β decay of ^{6}He [9-11] and ^{23}Ne [2, 12]. Only one measurement in the decay of ^{6}He [9] was performed with a relative precision at the level of 1%, yielding $a_{\beta\nu}=-0.3308(30)$ after inclusion of radiative and induced second class currents corrections [13]. To search for (or better constrain) tensor coupling contributions, new experiments using modern trapping techniques coupled to radioactive beams with high production rates are very promising. They provide new independent measurements, reduce instrumental effects like the scattering of electrons in matter, and allow the detection of the β particles and recoil ions in coincidence, thus providing a better control of systematic effects. Even if MOTs

have successfully been used with radioactive noble gas atoms in precision experiments [14, 15], they are efficiency limited for correlation measurements. This is not the case for ion traps [16, 17] which are suitable for any kind of singly charged ions. In this context, the WITCH setup being developed at ISOLDE-CERN to measure $a_{\beta\nu}$ in the β decay of ^{35}Ar is based on a Penning trap coupled to a retardation spectrometer [18, 19], and the LPCTrap installed at GANIL is a transparent Paul trap dedicated to correlation measurements [20, 21].

Concerning the nuclei of interest for such studies, the ^{6}He nucleus is particularly suitable for a β–ν angular correlation measurement: 1) it has a pure Gamow-Teller transition, 2) the decay involves a single branch to the ^{6}Li ground state, 3) its half life, $T_{1/2}$ = 807 ms, is in the range required for efficient trapping, and 4) a high production rate can be achieved by the SPIRAL source at GANIL. The LPCTrap setup was thus designed to allow an efficient trapping of light ions such as $^{6}He^{+}$.

2. The LPCTrap experimental setup

The experimental setup, installed at the low energy beamline LIRAT of the GANIL-SPIRAL facility, has already been described in detail elsewhere [20-22]. The radioactive $^{6}He^{+}$ ions were produced by a primary ^{13}C beam at 75 MeV/A bombarding a graphite target coupled to an ECR ion source. The beam was mass separated by a dipole magnet having a resolving power of $M/\Delta M$ ~ 250 and delivered to the LPCTrap at 10 keV through the LIRAT beamline. Even after mass separation, the largest fraction of the ~10 nA ion beam was composed of stable $^{12}C^{2+}$ ions. The typical $^{6}He^{+}$ intensity in the incident ion beam was 1.5×10^{8} s^{-1}, as measured by implanting a calibrated fraction of the beam on a retractable silicon detector.

The LPCTrap comprises a Radio Frequency Cooler and Buncher (RFQCB) for beam preparation [23], a short transport line with beam optics and diagnostics and the detection chamber containing the transparent Paul trap. The incident $^{6}He^{+}$ ions are first decelerated below 50 eV by the high voltage applied to the RFQCB platform, they are then cooled down with a 7×10^{-3} mbar pressure of H_2 buffer gas, and bunched close to the exit of the quadrupole. During this process, the $^{12}C^{2+}$ ions undergo singly charge exchange with H_2 molecules and are eventually lost on the walls of the RFQCB. The $^{6}He^{+}$ bunches are extracted from the RFQ at a repetition rate of 10 Hz, and reaccelerated up to 1 keV using a first pulsed cavity located at the entrance of the transport beamline. A second pulsed cavity reduces the kinetic energy of the ions down to 100 eV for an efficient injection into the Paul trap. The Paul trap, shown in figure 1, is made of six stainless steel rings. This trap geometry allows the application of suitable voltages for an efficient injection, and for the extraction of ions towards a micro-channel plate position sensitive detector (MCPPSD) dedicated to the ion cloud monitoring [20].

In the run described in this paper, an average of 700 ions were successfully trapped for each injection of an ion bunch, and the storage time of the ions in the trap was found to be ~ 240 ms, after accounting for the losses due to β decay. The RF voltage applied to the rings R1 and R2 was set to 120 V_{pp} at 1.15 MHz. During the first 25 ms of the trapping cycle, the ions confined in the transparent trap were further cooled down by elastic collisions with H_2 buffer gas at low pressure (typically 2×10^{-6} mbar). Once the thermal equilibrium is reached, the ion cloud has a final thermal energy kT ~ 0.1 eV and a diameter of ~2.4 mm (FWHM). After a 95 ms trapping duration dedicated to the β decay measurement, the ions were extracted toward the ion cloud monitor and replaced 5 ms later by a new bunch coming from the RFQCB.

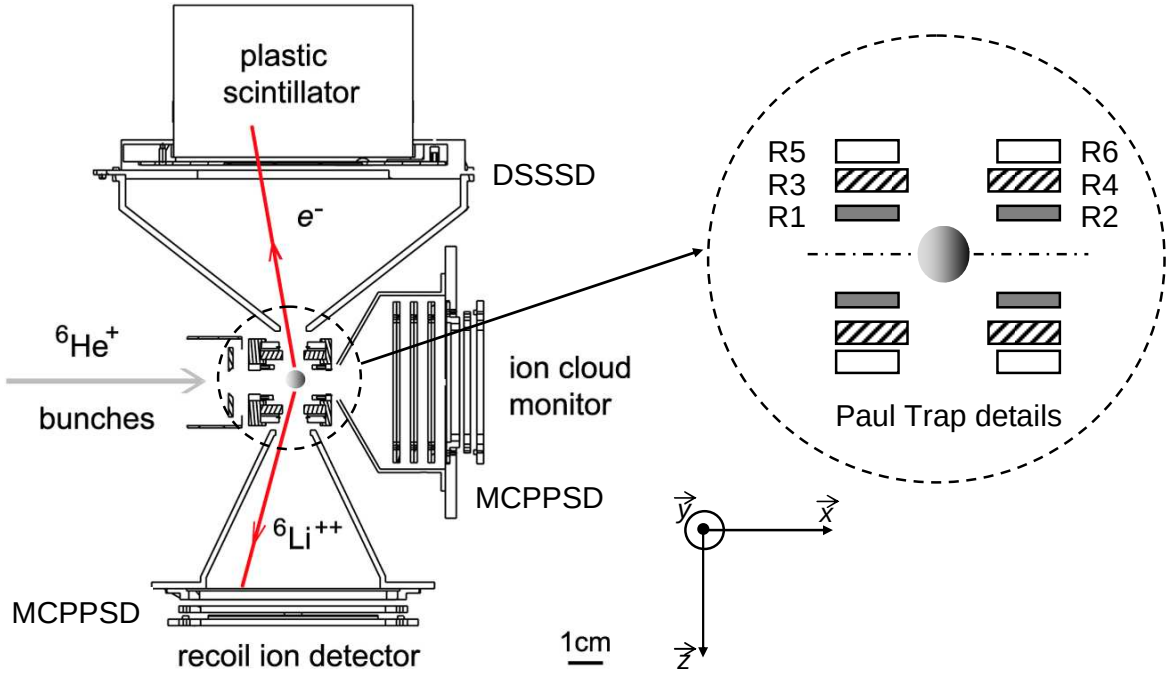

Figure 1. Top view of the detection chamber (see text). An enlarged view of the Paul trap is shown in the zoom. The six rings are labelled R1 to R6.

A telescope for β particle detection and a second MCPPSD are located 10 cm away from the trap centre in a back to back geometry. To prevent the detection of particles emitted by the ^{6}He atoms leaking from the RFQCB, thick stainless steel collimators are located in front of each detector. For ions decaying inside the Paul trap, the collimators also limit the detection efficiency of a full coincidence event to 0.15%. In order to avoid that the detection efficiency of the recoil ion detector depends on the ion incident angle and energy, the MCPPSD comprises a 90% transmission grid located 6 mm in front of the active surface of the detector. This grid is connected to the ground and, by applying a -4 kV voltage to the front face of the MCP, an additional kinetic energy of 8 keV is provided to the $^6Li^{2+}$ ions that are thus all detected with maximal efficiency. The performances of this detector are detailed in reference [24]. The β telescope is composed of a 60 × 60 mm^2 300 µm thick doubled sided silicon strip detector (DSSSD) for position readout, followed by a plastic scintillator coupled to a photomultiplier for the β particle energy measurement. This detector provides the trigger of an event and generates a start signal for the recoil ion time of flight (TOF) measurement between the center of the trap and the recoil ion MCPPSD. For each coincidence event, one records the positions of both particles, the recoil ion TOF, and the β particle energy. With the combination of these observables, the kinematics is over-determined, which makes possible the reconstruction of the antineutrino rest mass. As shown in section 4, appropriate cuts in the antineutrino mass spectrum provide a means to reduce background contributions in the TOF spectrum and the shape of the neutrino mass spectrum enables additional control of instrumental effects. Two additional parameters were also recorded for each detected event: the RF phase of the Paul trap for the off-line study of the RF field influence, and the time within the trapping cycle to select decay events from trapped ions already cooled down and at thermal equilibrium. The data presented here were collected at GANIL in 2006. A total of about 10^5 coincidence events have been recorded within 49 runs of typically 20 minutes duration. Preliminary results from this experiment have previously been reported [21].

3. Data analysis

Since the recoil ion energy distribution is the most sensitive observable to the β–ν angular correlation, we used the TOF spectrum of the recoil ions to extract $a_{\beta\nu}$. The analysis is based on the comparison between the experimental TOF spectrum and those obtained for two sets of realistic Monte Carlo (MC) simulations considering pure axial ($a_{\beta\nu}$ = -1/3) and pure tensor ($a_{\beta\nu}$ = +1/3) couplings. In a first step, the experimental data are calibrated and corrected for the identified sources of background, also

included in the MC simulations. Then, $a_{\beta\nu}$ is deduced from an adjustment of the experimental TOF spectrum with a linear combination of the two sets of simulated decays obtained for axial and tensor couplings (figure 2).

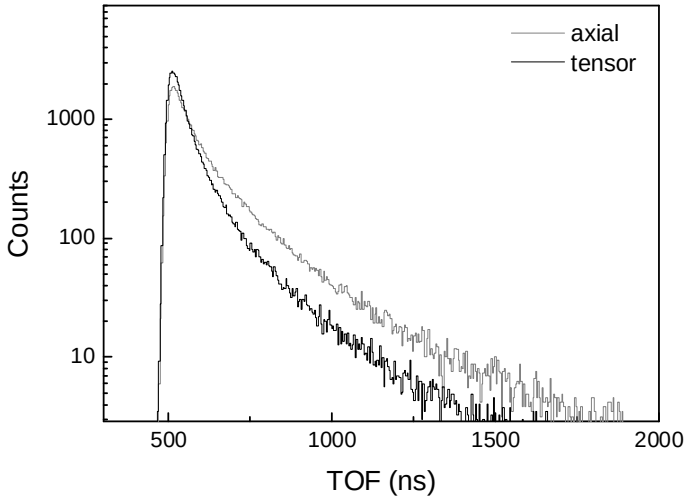

Figure 2. Monte Carlo simulations of the time of flight spectra expected under the conditions of this experiment (including, among others, the detection of the recoil ion in coincidence with the β particle) for pure axial ($a_{\beta\nu}$ = -1/3) and pure tensor ($a_{\beta\nu}$ = +1/3) couplings.

All the relevant instrumental effects, including the detectors response function and geometry, the trap RF field influence, the ion cloud space and velocity distributions, the shake off ionization of the recoil ion, and the scattering of the β particles, are implemented in the simulations. Finally, the uncertainties on each parameter of the simulations and calibrations are evaluated as well as their associated contribution to the determination of $a_{\beta\nu}$.

3.1. Monte Carlo simulations

The MC simulations performed for this analysis include the following modules: 1) an event generator for the β decay kinematics considering pure axial and pure tensor couplings, 2) a realistic simulation of the trapped ion cloud, 3) propagators for the β particles and recoil ions, 4) the response functions of the detectors, and 5) event generators for the sources of background.

3.1.1. β decay dynamics. The evaluation of the angular correlation parameter takes into account radiative corrections [13, 25]. We have used the formalism described by Gluck [13], based on the work of Sirlin [26] to calculate, to first order in α and on an event by event basis, the change in the kinematics due to the virtual and real photon emission during the decay process. The implementation of such corrections in the data analysis has been checked by comparing our results with those of the table 1 in reference [13]. It turns out that such corrections are at the 1% level on the value of the correlation parameter. In view of the limited statistics of this run, no explicit sensitivity on radiative corrections was observed. Other recoil-order corrections in the beta-neutrino correlation distribution [27, 28] were found at the 0.1% level [13] for the Johnson's experiment [9]. These were thus neglected in the present work. It was also assumed that the Fierz parameter b of equation (1) is equal to zero. However, if this condition is relaxed, this leads to a renormalization of $a_{\beta\nu}$ that makes it slightly dependent of E_e. The actual quantity that is determined experimentally is then

$$\tilde{a}_{\beta\nu} = a_{\beta\nu} / (1 + \left\langle b \frac{m}{E_e} \right\rangle) \qquad (7)$$

where the brackets $\langle\ \rangle$ stand for a weighted average over the observed part of the β spectrum.

The shake off ionization of the recoil ions has also been taken into account in the MC simulations. This ionization is mainly caused by the sudden change of the electric charge of the nucleus following β decay and results in $^6Li^{3+}$ ions production. The effect of the RF electric field of the Paul trap and of

the MCPPSD post-acceleration field is slightly different for $^6Li^{3+}$ ions than for $^6Li^{2+}$ ions. For $^6Li^{3+}$ ions, the leading edge of the TOF spectrum is shifted toward shorter TOF values by a few ns, and the rising time is enlarged by a few percent. For the present analysis, the shake off ionization probability of $^6Li^{2+}$ ions has been calculated in the sudden approximation limit, and found to be 0.02334 + $0.00004 \times E_{RI}$ [29] where E_{RI} is the ion recoil energy in keV. The maximum recoil energy being 1.4 keV, the energy dependent term can be neglected here. This ionization probability is in perfect agreement with previous calculations of Wauters and Vaeck [30]. To account for the shake off ionization process, we included a production of 2.3% of $^6Li^{3+}$ ions in the MC simulation.

3.1.2. Trapped ion cloud. It has previously been shown [31] that the TOF spectrum of recoil ions strongly depends on the size of the ion cloud. Simulations of the trapped ions trajectories in the Paul trap have thus been performed using the SIMION8 software package [32]. The geometry of the electrodes and of the surrounding elements was included, and the RF trapping voltages applied in the simulations were those recorded during the experiment using an oscilloscope probe. The collisions between the trapped ions and the H_2 buffer gas molecules were also described at the microscopic level using realistic interaction potentials [33]. The position and velocity distributions at thermal equilibrium as a function of the RF phase were then extracted from the simulation of the ion motion. The mean thermal energy of the ion cloud averaged over a full RF period as given by this simulation is kT_{sim} = 0.09 eV. To consider possible cloud temperatures slightly different than the one predicted by the simulation, the reduced mean square of the cloud space and velocity distributions obtained for a given RF phase can be scaled by an arbitrary factor, α_T. By varying this scaling factor in the analysis, it is thus possible to use the cloud temperature given by independent measurements and to estimate the systematic error on $a_{\beta\nu}$ due to the uncertainty on the ion cloud temperature measurement. We used the thermal energy value kT_{sim} = 0.107(7) eV, provided by off-line measurements [31]. These measurements, performed for different ion cloud densities in the Paul trap, have also shown that space charge effects could be neglected in the simulation.

3.1.3. Decay particles trajectories and detection. In the MC simulations, the initial RF phase at the decay time is randomly sampled. The initial ion position and velocity are sampled accordingly to this RF phase and to the chosen cloud temperature. The recoil ions trajectories are then simulated using SIMION8 within the oscillating RF field of the Paul trap, from the decay vertex, up to a plane located 40 mm beyond the entrance of the collimator. The ions are then in a free field region and the ion trajectories can be extrapolated onto the plane corresponding to the post-acceleration grid of the MCPPSD. The additional TOF between the post-acceleration grid and the front face of the micro-channel plate assembly is calculated analytically. The time and position resolutions of the MCPPSD [24] are about one order of magnitude smaller than the bin widths chosen for the TOF and the recoil ion position spectra (respectively 4 ns and 1 mm). They have been neglected here.

The associated β particle is not affected by the RF field and is therefore analytically propagated from the decay vertex up to the DSSSD, with the only condition that the particle can enter the collimator. For the energy range of the β particles selected for the analysis (from 500 keV to 3508 keV), the energy deposited in the silicon detector E_{si} is weakly dependent on the incident energy, as seen in figure 3. In the simulation, E_{si} is randomly sampled according to an arbitrary probability function adjusted on the experimental results:

$$P(E_{si}) = A_0 \times \exp^{-\frac{(Z+\exp^{-Z}-1)}{A_3}} \tag{8}$$

$$\text{with} \quad Z = \frac{(E_{si} - A_1)}{A_2} \tag{9}$$

where the parameter A_1 corresponds to the energy deposited with maximal probability, and A_2 and A_3 are shape parameters. The use of this distribution avoids the integration needed in a Landau distribution, and nicely reproduces the experimental data. The weak dependence on the incident energy, yielding a shift of about 10 keV for the lowest values of E_{scint}, is neglected here. However, the variable average thickness of silicon associated to the incident angle of the particle is taken into account using a linear scaling.

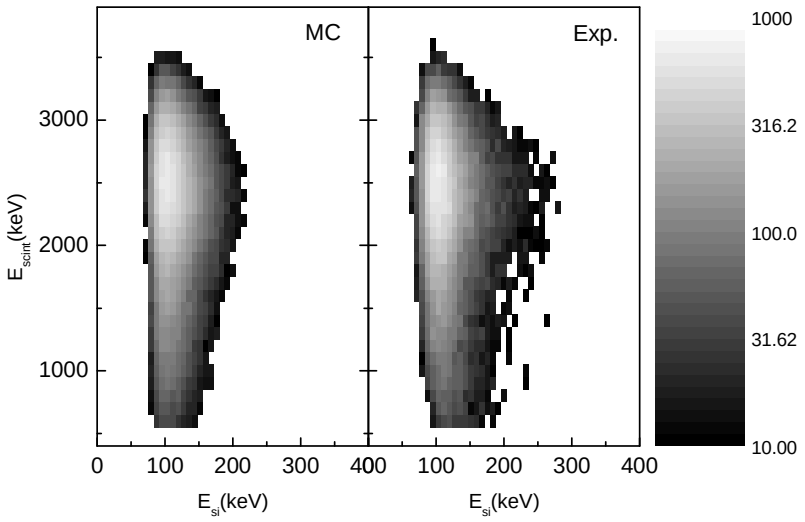

Figure 3. Energy deposited in the scintillator versus the energy deposited in the silicon detector for simulated coincidence events (left panel) and experimental data (right panel). The MC simulation is normalized to the experimental data.

The response function of the plastic scintillator included in the simulation follows a normal distribution. According to the statistics of electrons produced by the cathode of a photomultiplier, the resolution on the energy deposited E_{scint} can be expressed as

$$\sigma(E_{scint}) = \sqrt{{\sigma_{elec}}^2 + {\sigma_{ph}}^2 \times E_{scint}} \qquad (10)$$

σ_{elec} being the reduced mean square (RMS) of the electronic noise, and σ_{ph}, the RMS due to the photo-electrons statistics at 1 MeV. The time resolution of the detector, smaller than 1 ns, is neglected in the analysis.

In the simulation, the telescope and the MCPPSD can both be moved around their nominal positions and orientations to study the associated systematic effects. The backscattering of β particles on the detectors and on other structures of the detection chamber are treated independently.

3.1.4. β scattering. The β scattering can be a significant source of systematic errors. The backscattering probability on the silicon detector depends on the β incident energy which then affects the β energy distribution of the detected events and thus the TOF distribution of the recoil ions. In a similar way, β particles emitted in another direction can be scattered towards the detector by the electrodes of the Paul trap. To account for these effects, MC simulations using the GEANT4 toolkit [34] have also been performed. The geometry of the detection chamber has been simulated including the most relevant volumes and materials (figure 4). The β scattering is natively included in GEANT4. The dynamic electric field from the RF trap has been implemented [35] using the potential maps provided by SIMION8.

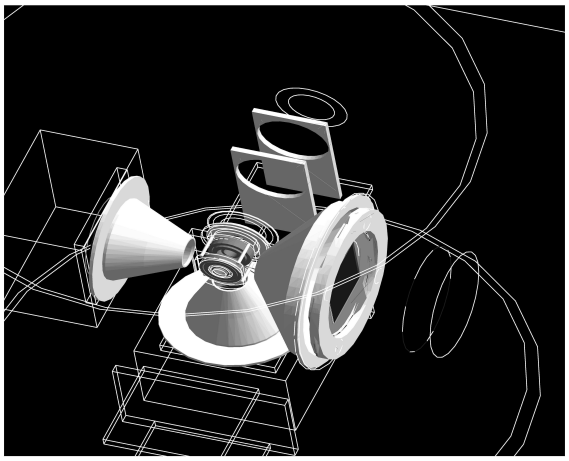

Figure 4. Example of a GEANT4 visualization of the detection chamber.

The backscattering probability on the DSSSD, as a function of the incident energy and angle of the β particle, was determined in a first step. To account for missing events due to backscattering, this probability function was embedded in the β telescope response function.
A second simulation was dedicated to estimate the yields and characteristics of detected events tagged with at least one scattering process in the detection chamber ("scattered" events). In this simulation, the β particles were emitted from the Paul trap in a 4π solid angle, and the decay kinematics was sampled assuming a pure axial coupling. In the analysis, the "scattered" events obtained in the simulation are treated as a source of background and subtracted from the experimental data.
3.1.5. Background simulation. Within the 100 ms trapping cycle, the ions were kept confined in the trap during 95 ms. The remaining time after the ion cloud extraction was too short to record a sufficiently large fraction of background events and those had then to be simulated for this run.
The main source of background is due to false coincidences ("accidentals"), corresponding to the detection of uncorrelated particles on the β telescope and on the MCPPSD. This background appears as a flat contribution in the TOF spectrum and can easily be subtracted. However, it is valuable to perform a full simulation of such events, to correct for their contributions to other observables like, for instance, the particle positions and the energy deposited in the β telescope. During the experiment, the triggering of the MCPPSD was largely dominated by hot H_2 molecules leaking from the RFQCB, as established by run tests performed without the $^6He^+$ beam for different H_2 buffer gas pressures. This background is thus uniformly distributed on the entire surface of the detector. By comparing the counting rate of the β telescope with the number of trapped ions, it was deduced that about 90% of the β particles detected as singles (without any condition on the MCPPSD) were originating from neutral ^{6}He atoms, also leaking from the RFQCB. On the β telescope, the position and the energy deposited are thus obtained by simulating the decays of ^{6}He atoms uniformly distributed over the whole volume of the detection chamber. The TOF corresponding to the "accidentals" is randomly sampled over the coincidence time window.
For a small fraction of the ^{6}He atoms decaying in the chamber volume, the recoil ion can be detected on the MCPPSD, in coincidence with its associated β particle. This constitutes another source of background events labeled "out-trap" events in the following. Their contribution to the TOF spectrum in the region of the fit can bias the measurement. They were included in the simulation, assuming a decay process with pure axial coupling.
A third source of background is due to ^{6}He atoms, trapped in the micro-channels of the recoil ion detector due to their large length to diameter ratio [24]. The recoil ions produced inside the micro-channels can be detected with detection efficiencies up to 25% for recoil energies larger than 1 keV, and the β particles emitted with an appropriate angle can be detected by the β telescope. These events are identified by a time of flight peaked close to zero, and they can easily be isolated from the β decay data.

3.2. Detector calibrations
3.2.1. Time of flight and recoil ion detector. A careful calibration of the time digitalization chain (a time-to-amplitude converter coupled to an amplitude-to-digital converter) was performed to correct for linearity defects. The calibration curve was obtained using a time-calibrator (TC) (model 462 from ORTEC) providing periodic stop pulses separated by 10 ns over a 10.24 μs time window. The TC absolute accuracy for the full scale is 0.5 ns.

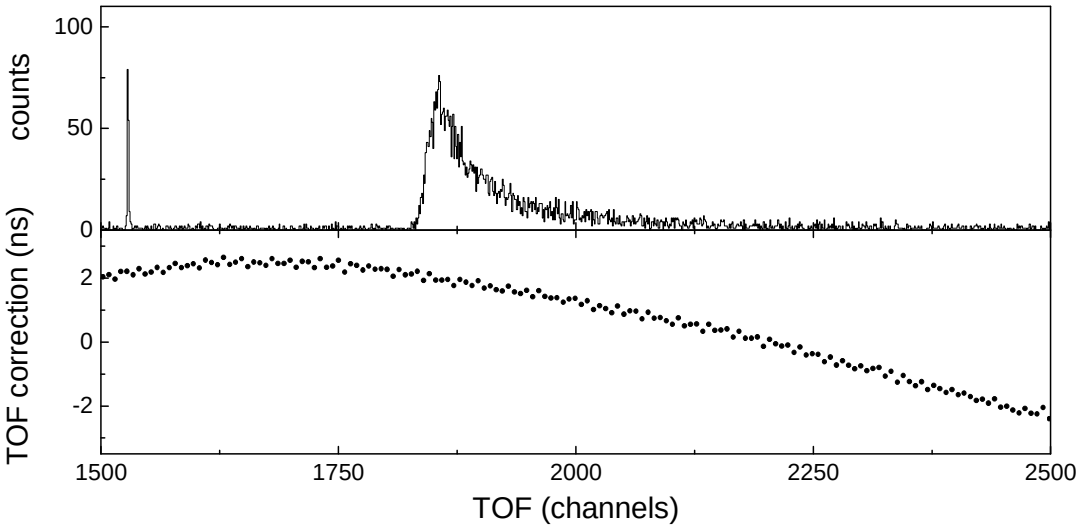

Figure 5. *Top:* Raw TOF spectrum for a typical run. *Bottom:* TOF deviation from a linear fit of the calibration points obtained with the time-calibrator. On the horizontal scale, 1 channel corresponds to 1.569 ns.

The deviation from a linear fit of the calibration data points, within the time window of interest, is shown in figure 5 and was accounted for in the analysis. To check the results obtained with the time-calibrator, two desynchronized clocks have been set up to generate start and stop signals randomly. This should ideally result in a uniform time distribution. The time spectrum provided by these clocks was normalized to 1 count per channel and compared to the relative variation of the calibration slope obtained with the time calibrator. Both calibration techniques were found in good agreement.

An ^{241}Am calibration source was inserted right after the experiment at the centre of the Paul trap. Coincidences between α particles emitted toward the MCPPSD and 59.5 keV γ rays detected by the plastic scintillator were recorded during a few hours. The time interval between the γ detection and the electronically delayed detection of the α particle was measured under the same running conditions than for the ^{6}Li ions TOF measurement. The time spectrum of these coincidence events (figure 6) allowed an accurate determination of the absolute time reference corresponding to the simultaneous triggering of the β telescope and of the MCPPSD. The sharp peak near channel 1500 in the TOF raw spectrum (figure 5, upper panel), was then unambiguously attributed to "simultaneous" triggers of both detectors. Using the information given by the DSSSD position and the energy deposited in the β telescope, these events were identified as due to ^{6}He atoms decaying in the recoil detector MCPs. The position of this peak has been fitted for each run in order to control the stability of the system and to correct for slow drifts which remained bellow 1.5 ns for the duration of the experiment. The TOF resolution of $\sigma = 0.8$ ns could also be deduced from the RMS of this peak.

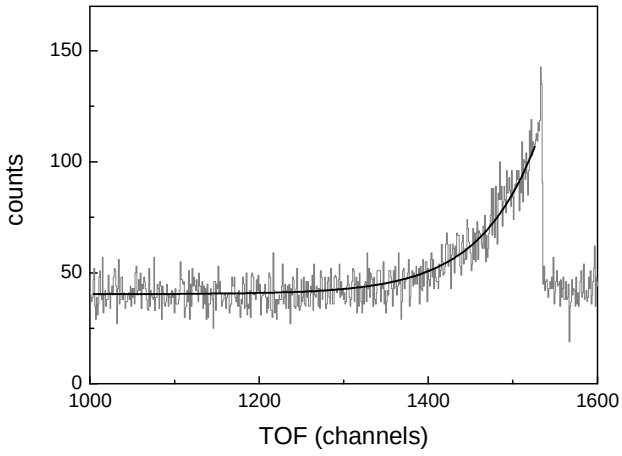

Figure 6. Time spectrum of coincidences between α particles and 59.5 keV γ rays emitted by a ^{241}Am calibration source. The fit of the data by an exponential decay

curve corresponds to a half-life of 69.4(2.5) ns for the excited level in the ^{237}Np daughter nucleus, in perfect agreement with the reference data [36].

The MCPPSD readout involves six parameters: the charge and time of the signal collected on the cathode of the MCPs, and the time difference between this signal and the four signals collected on the two delay line anodes. For a proper reconstruction of the position, several conditions were applied, like a minimal charge collected on the MCPs, and filters on the sum of time differences for each delay line [24]. The position calibration of the MCPPSD was then performed by adjusting the reconstructed position of the uniform background, due to H_2 molecules, to the nominal active diameter of the detector. Since the spatial distribution of the recoil ions collected by the detector is very weakly sensitive to the value of $a_{\beta\nu}$ (see figure 15), this calibration in position of the MCPPSD was then refined by fitting the experimental position spectra with the simulated ones. The detector spatial resolution of 110 μm and the position reconstruction accuracy of about 240 μm were measured in a previous study of the detector [24].

3.2.2. The β telescope. The plastic scintillator has first been roughly calibrated using the Compton edges obtained with ^{22}Na, ^{137}Cs, and ^{54}Mn calibration sources, and the Compton edges of ^{40}K and ^{208}Tl background present in the experimental area. The corresponding energies cover a range between 340 keV and 2380 keV, with a relative uncertainty of about 5% on the deposited charge associated to each Compton edge. With this coarse calibration, the energy resolution at 1 MeV was found to be about 10% RMS and the response of the detector was found to be non linear. Since no calibration point is available above 2380 keV with conventional calibration sources, the end point of the β energy spectrum in ^{6}He decay has been included. The calibration curve of the detector was then obtained by fitting the calibration points with a rational function

$$E_{sc\,\mathrm{int}} = \frac{P_1 Q^2 + P_2 Q + P_4}{Q - P_3} \tag{11}$$

where Q is the charge collected on the photo-multiplier anode and $P_{1,2,3,4}$ are free parameters of the fit. This function reproduces both, the almost linear behaviour of the detector for the low energy part as well as the charge saturation occurring for signals of higher amplitude (figure 7).

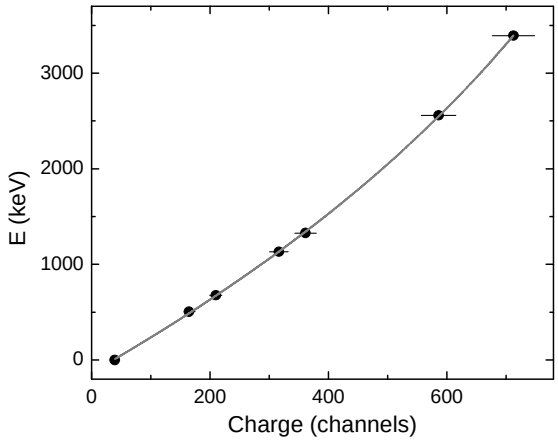

Figure 7. Calibration points of the energy deposited in the plastic scintillator (black dots) adjusted with a rational function (gray line).

In order to obtain a more precise calibration, we used the β energy spectrum provided by the simulation for coincidence events (assuming pure axial coupling), and compared it to the calibrated experimental one using a chi-square test. In the procedure, three parameters could be adjusted: i) the charge corresponding to the five Compton edges could be altogether varied in a range of $\pm 5\%$, ii) the charge corresponding to the end point of the ^{6}He β energy spectrum was left free, and iii) the detector resolution σ_{ph} (RMS at 1MeV due to photo-electrons statistics) could be adjusted between 8.5% and 11.5% by steps of 0.5%. Each combination of calibration points resulting from the adjustment of the first two parameters (points i, and ii) was fitted with equation 11 to build an experimental spectrum of the energy deposited in the scintillator (E_{scint}). These experimental spectra were then compared to a set

of 7 simulated ones with detector resolutions at 1 MeV, σ_{ph}, ranging from 8.5% to 11.5%. The best chi-square was obtained using the calibration curve displayed in figure 7 and a detector resolution σ_{ph} = 10%. Finally, to check for a possible bias of this method due to the pure axial coupling assumption in the simulation, the values of $a_{\beta\nu}$ were varied by 10% to $(-1/3)\times 1.1$, and $(-1/3)\times 0.9$. For the three values of $a_{\beta\nu}$, the best chi-square has been obtained with the same set of parameters, which demonstrates that the calibration method is not sensitive to $a_{\beta\nu}$. The comparison between the experiment and the simulation with $a_{\beta\nu}$ = -1/3 is shown figure 8 (top panel). For each bin, the normalized residuals

$$\chi = (n_{\exp} - n_{fit}) \Big/ \sqrt{n_{\exp}} \tag{12}$$

are displayed in the lower panel.

Each of the 120 strips of the DSSSD was calibrated independently, and the procedure was done run by run to account for small drifts of the charge pedestals. For this, we first used events in singles (no recoil ion detection required) to obtain a significant statistics. Three filters were applied: 1 MeV deposited in the scintillator, a minimal charge deposited in a strip (to reject electronic noise signals), and no charge deposited in the closest neighbours. This provided a relative energy calibration of each strip. In a second step, the absolute calibration in energy was done by comparing the mean collected charge with the mean energy deposited obtained with a GEANT4 simulation using events in coincidence. To obtain the mean collected charge, a more complex validation procedure was applied: a minimal charge threshold for each channel, a clustering of adjacent hits for each side, a second minimal charge threshold for the clusters, and a minimal difference between the charges collected on the two sides of the DSSSD.

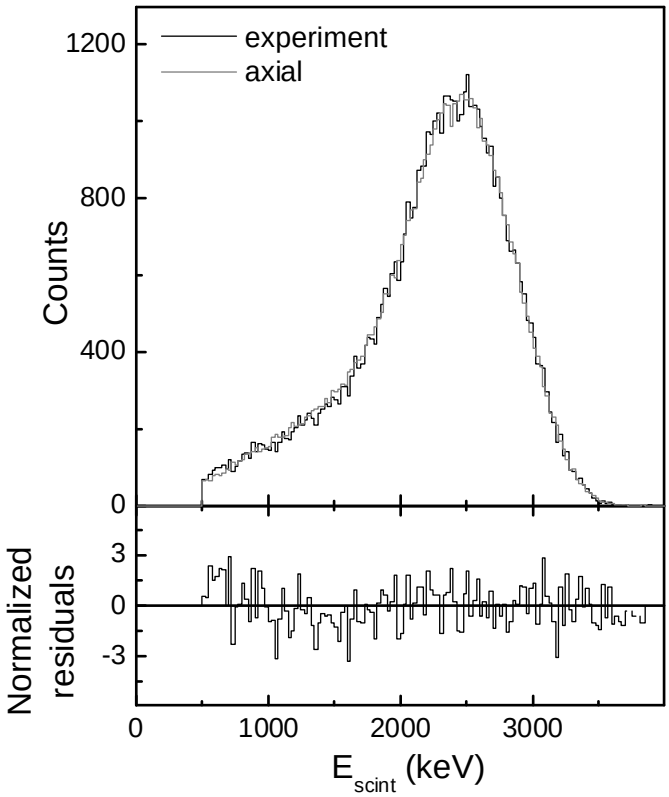

Figure 8. *Top panel*: energy deposited in the scintillator. The black line corresponds to the calibrated experimental spectrum, the gray curve to the simulated one using $a_{\beta\nu}$ = -1/3. *Low panel*: normalized residuals between the two spectra.

4. Results

4.1. Reliabilities of background subtraction and simulation

The TOF spectrum obtained for valid coincidence events is displayed in figure 9. The selected events are conditioned by: a 500 keV energy threshold on the energy deposited in the scintillator, a time

within the trapping cycle between 25 and 95 ms, and a valid reconstruction of the positions in both the DSSSD and the MCPPSD. The simulation of the “accidentals” background contribution was normalized by integrating the experimental spectrum between 3 and 4 μs. The simulation of the “out-trap” contribution was then normalized using the counts in excess above the accidentals, observed just before the leading edge of the TOF spectrum. It is to be noticed that measurements of the background performed later in a new run, nicely confirmed that the shape of the "out-trap" events was properly described in the simulation. The yield of “scattered” events is provided by the GEANT4 simulation. In the TOF window up to 4 μs, the “scattered”, “out-trap”, and “accidentals” events represent respectively 4.5%, 2.6%, and 7.3% of the total number of events. These background contributions and the TOF obtained for $a_{\beta\nu}$ = -1/3 are summed and compared to the experimental spectrum in figure 9.

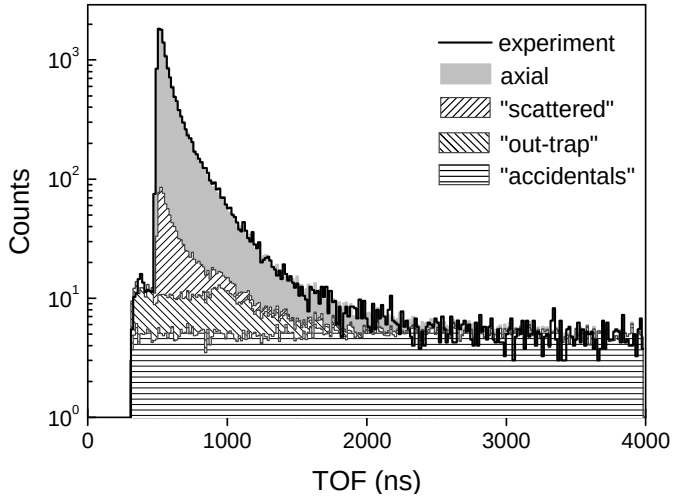

Figure 9. Experimental time of flight spectrum (black line) compared to the simulated one (grey area) in the pure axial case, including the different simulated background contributions after normalization (see text for details).

By considering the β decay vertex as a point like source at the centre of the Paul trap, the recoil ion TOF and position can be used to determine the three components of the recoil ion momentum. The full momentum vector of the β particle can be, in a similar way, deduced from the energy deposited in the β telescope and the position on the DSSSD. This provides the possibility to reconstruct the antineutrino invariant mass:

$$m_\upsilon^2 = E_\upsilon^2 - p_\upsilon^2 \tag{13}$$

As mentioned in section 3.1, the background sources are fully simulated in order to generate all the parameters recorded in the real experiment. The reconstruction of the antineutrino mass can therefore be applied to the simulated background events. Figure 10 shows the antineutrino invariant mass spectra obtained for the experimental and simulated events. The main peak is well reproduced by the simulations. The shape and position of this peak depend on all the inputs included in the simulations (background, detector response functions, geometries, size of the ion cloud, trap RF field, etc…), and the good agreement obtained here provides a high level of confidence in the analysis procedure.

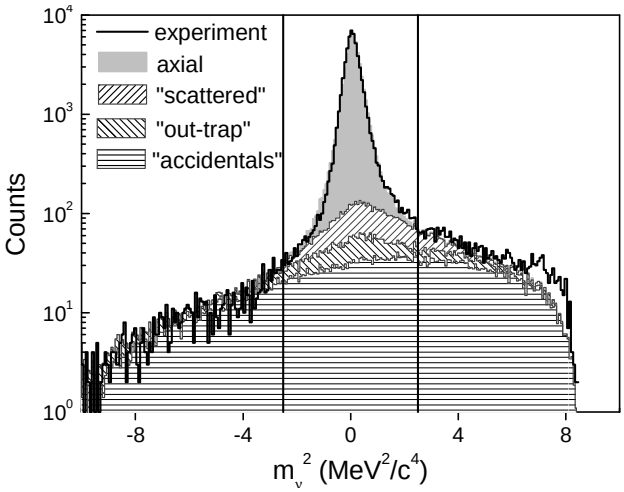

Figure 10. Antineutrino invariant mass spectra for the experimental data, the simulation in the pure axial case, and the simulation of background events.

For $\left|m_\upsilon^2\right| > 2.5\,\mathrm{MeV}^2/\mathrm{c}^4$, where only the background events contribute, the experiment and the simulations are also in good agreement. This shows that the relevant background sources have been well identified and properly taken into account. The small discrepancy above 6 $\mathrm{MeV}^2/\mathrm{c}^4$ is due to an excess of experimental "accidentals" with a very low energy deposited in the scintillator and in the DSSSD. They are most likely caused by electronic noise triggering the β telescope. These events, as well as 40% of the total background, are suppressed by applying a cut between -2.5 and 2.5 $\mathrm{MeV}^2/\mathrm{c}^4$. The effect of the m_ν^2 cut is clearly seen in figure 11 which shows event distributions as a function of the recoil ion TOF and of the energy deposited in the scintillator after background subtraction. The two experimental spectra built with and without the m_ν^2 cut are compared to the simulation with axial coupling. The same correlation between the recoil ion TOF and the energy deposited in the scintillator can be observed in the simulation and the experimental data. The statistical fluctuations due to background subtraction observed (figure 11, (a)) in the region forbidden by the three body decay kinematics, are strongly reduced using the m_ν^2 filter (figure 11, (b)).

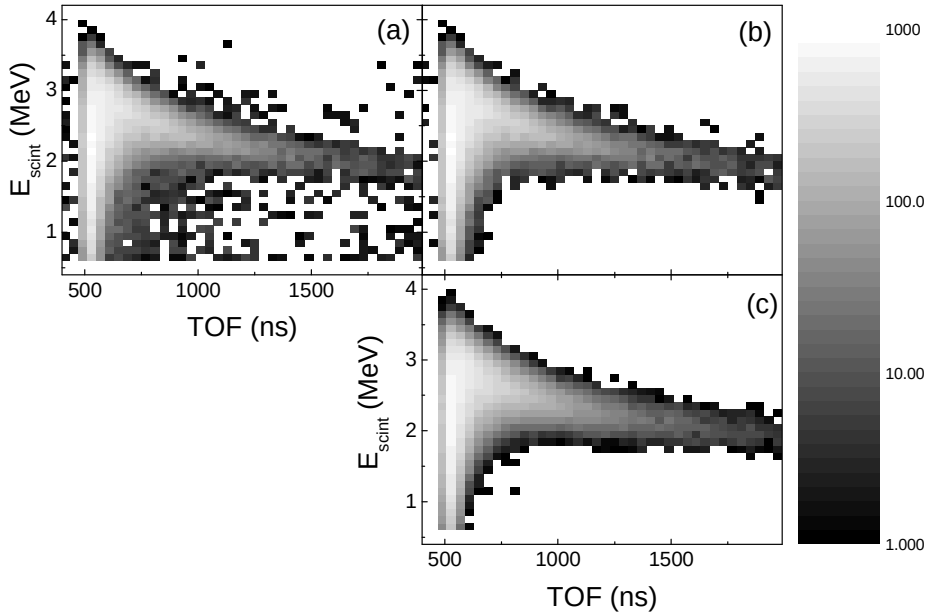

Figure 11. Event distributions as a function of the recoil ion TOF and deposited energy in the scintillator E_{scint}. Experimental data without (a) and with (b) m_ν^2 filter compared to the simulation (c).

A relevant input in the simulation is the propagation of the recoil ions in the presence of the trap RF field. It is however difficult to obtain an independent quantitative test of the quality of the simulations, in particular because the trapping conditions were not changed during this run. The effect of the RF field on the ions trajectories can be evidenced by looking at the leading edge of the TOF spectra obtained for different selections of RF phase (figure 12). The simulations were carried out assuming the ion cloud thermal energy was kT_{sim} = 0.107(7) eV (see below) and the neutrino mass filter described here above was applied to the experimental data. The comparison with the experiment shows that the effect of the RF field is properly reproduced by the simulation. Although such comparison is qualitative, it provides additional confidence on the simulation. A similar comparison, looking also at the leading edge of the TOF spectra, but using higher statistics from a new run [37] showed that the simulation properly reproduces fine effects in the differences between the leading edges.

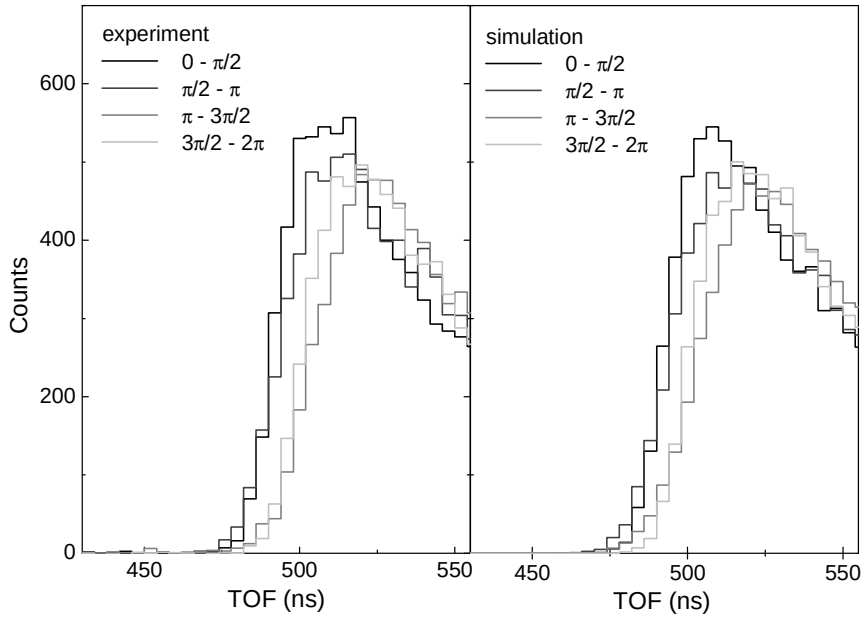

Figure 12. Leading edge of the TOF spectrum sorted as a function of the trap RF phase for experimental data (*left*) and simulations (*right*). The m_ν^2 filter and the background subtraction were previously applied to the data.

4.2. Statistical error

After applying an event selection for $\left|m_\upsilon^2\right| < 2.5\,\mathrm{MeV^2/c^4}$ and after background subtraction, the experimental TOF spectrum is adjusted with a linear combination of the time of flight spectra simulated using pure axial and pure tensor couplings (figure 13, left panel). Three parameters were left free in the fit: the value of $a_{\beta\nu}$, the total number of events, and the distance d_{MCPPSD} between the MCPPSD detection plane and the centre of the Paul trap. The range in TOF selected for the fit is indicated by the vertical lines. The experimental data have first been split randomly in four independent sets, and the corresponding TOF spectra fitted by changing the upper limit of the fitting range. No significant dependency has been found. Contours of constant χ^2 in the plane of parameters d_{MCPPSD} and $a_{\beta\nu}$ are shown on the right panel in figure 13. The result from the fit leads to $a_{\beta\nu}$ = - 0.3335 ± 0.0073, and d_{MCPPSD} = 100.255 ± 0.011 mm. The nominal value for this distance is 100.0 mm with a positioning uncertainty of 0.5 mm. The minimum chi-square χ^2_{min} = 96.6 for 105 degrees of freedom corresponds to a P-value of 0.71 which indicates a very good agreement between the data and the fitted function. The error is purely statistical. The data have also been split in four successive sets of equivalent statistics and independently analyzed. The results obtained for the four sets are statistically consistent, and their weighted mean value is the same than the value obtained by fitting the sum of all the data.

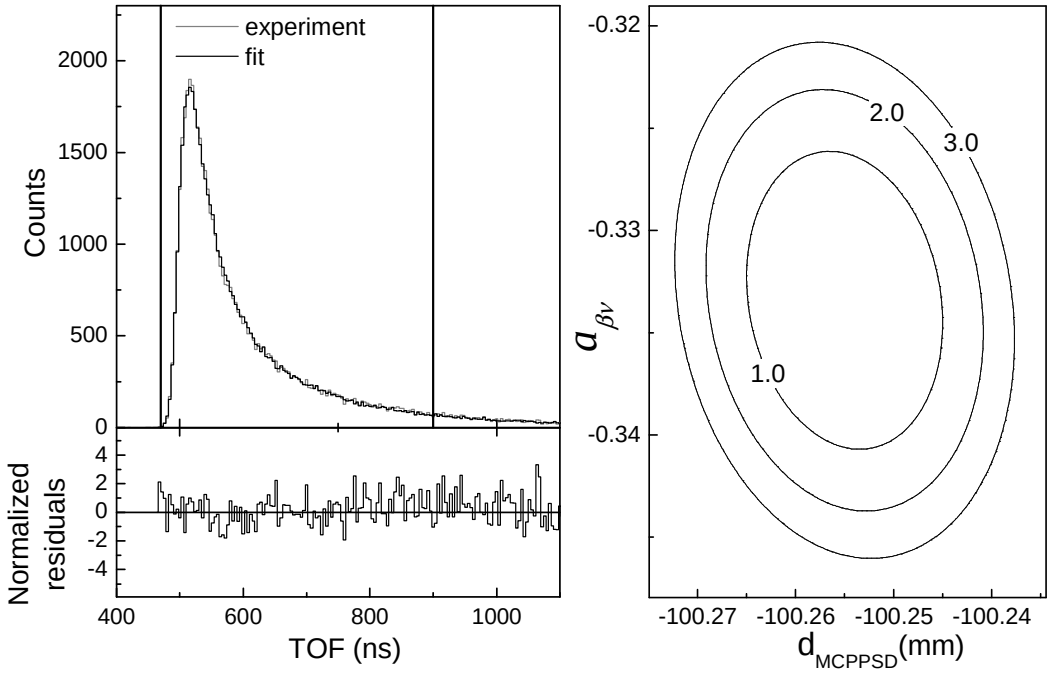

Figure 13. *Left panel:* Fit of the experimental spectrum (upper panel). The range of the fit function is indicated by vertical lines. The normalized residuals are plotted in the lower panel. *Right panel:* projection on the plane of parameters d_{MCPPSD} and $a_{\beta\nu}$ of the computed contours for (χ^2 - χ^2_{min}) values = 1, 2, and 3.

4.3. Systematic uncertainties

To estimate the systematic uncertainty, the contributions from all effects listed in table 1 have been studied. For most of the sources, the label "present data" in the column "Method" of table 1 indicates that the parameters and their uncertainties were determined by fitting the experimental data with the MC simulation (assuming a pure axial coupling). In each case, it was verified that the sensitivities of these parameters to the value of $a_{\beta\nu}$ taken as input were negligible at our level of precision. The associated uncertainties on $a_{\beta\nu}$ were then deduced from the changes in the $a_{\beta\nu}$ values resulting from the fit of the experimental TOF spectrum while varying the parameters in the MC simulation.

It was found that the $a_{\beta\nu}$ value resulting from the fit strongly depends on the trapped ion cloud size and temperature used in the MC simulation (figure 14). This motivated an independent measurement of the ion temperature using an off-line source of $^6Li^+$ [31], performed under identical running conditions than those in the $^6He^+$ experiment in terms of trap RF voltage, gas pressure in the trap chamber and number of trapped ions. A relative precision of 6.5 % was obtained which constitutes the dominant contribution to the systematic error on the value of $a_{\beta\nu}$. It is to be noticed that the temperature of the ion cloud can also be included as a free parameters of the TOF spectrum fit function, as shown in [37]. With the limited statistics of the present data, such a procedure leads to an uncertainty on $a_{\beta\nu}$ comparable to the one obtained using off-line measurements and was therefore not followed here. However, for runs of larger statistics, this would allow to improve the precision on both the cloud temperature and $a_{\beta\nu}$.

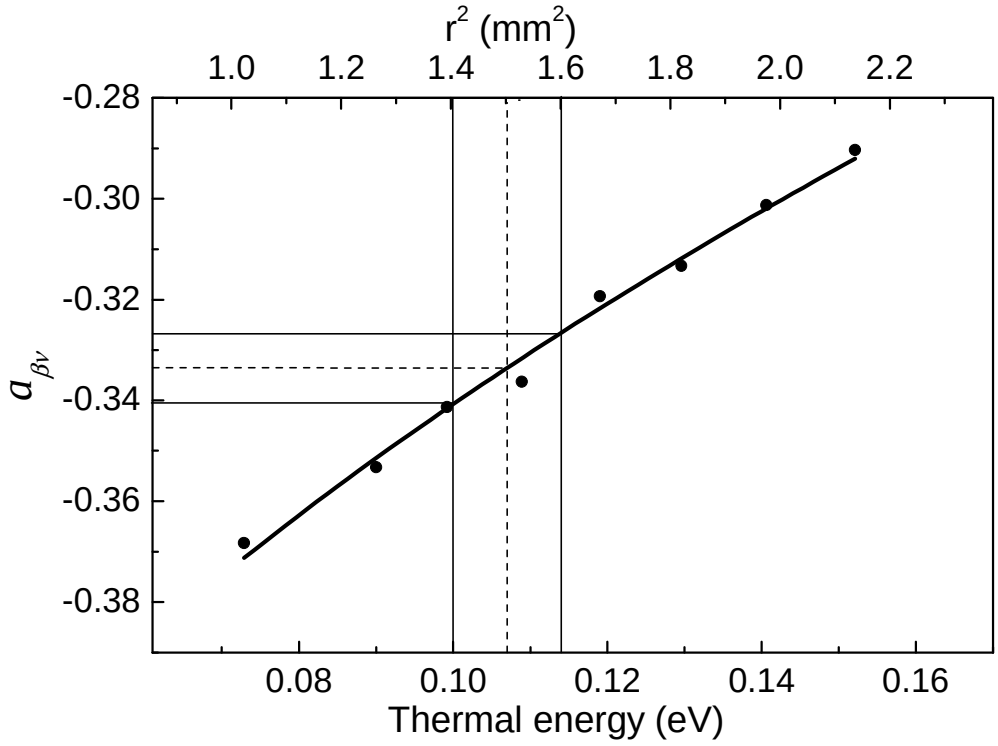

Figure 14. Values of the correlation coefficient resulting from the fit procedure as a function of the ion cloud thermal energy, kT, and of the ion cloud square radius, r^2, where r is the RMS of the spatial distribution in the Paul trap radial plane. The dashed and solid lines correspond respectively to the central value and the 1σ uncertainty of the off-line temperature measurement.

In order to precisely determine the orientation of the MCPPSD, four sets of events corresponding to recoil ions detected respectively in the right side, left side, upper side and lower side of the MCPPSD were selected to build the associated TOF spectra. The tilt angles around the *ox* and *oy* axis, $\theta x_{\mathrm{MCPPSD}}$, $\theta y_{\mathrm{MCPPSD}}$, and their uncertainties given in table 1, were obtained by fits of the leading edge of these TOF spectra with four sets of simulated events, sorted with the same selection filters. The chi-square minimization was performed for TOF shorter than 520 ns.

The positions of the DSSSD and of the MCPPSD in their detection planes were determined by fitting the *x* (horizontal position) and *y* (vertical position) experimental profiles. The best fits shown in figure 15 provide the detectors offsets in the detection planes, the refined calibration in *x* and *y* of the MCPPSD, and the distance d_{DSSSD} between the silicon detector and the centre of the Paul trap. The systematic error on $a_{\beta\nu}$ due to the uncertainties on the DSSSD position in the detection plane was found to be negligible.

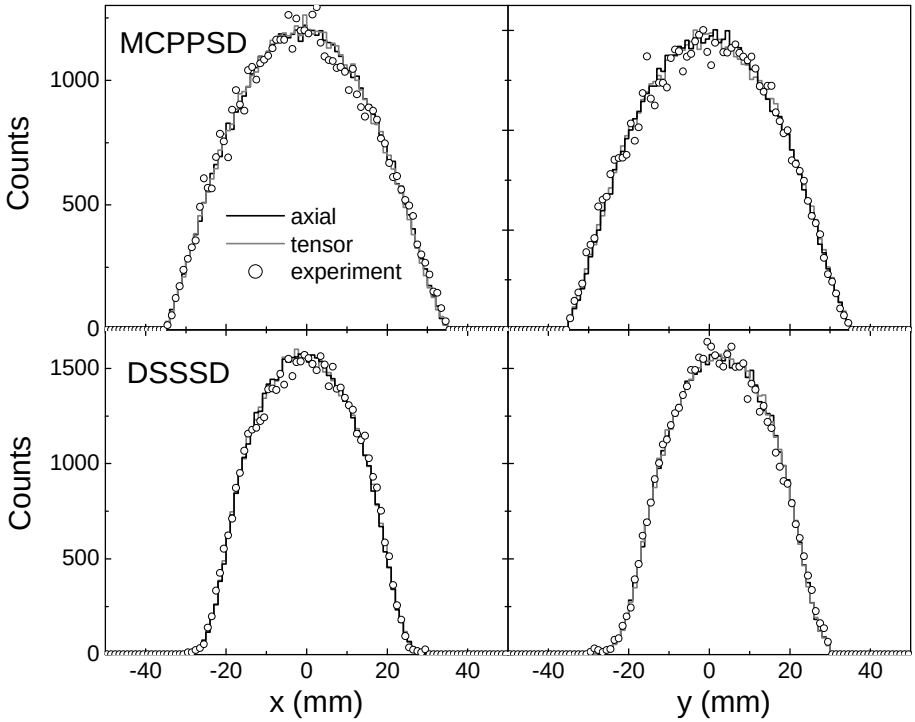

Figure 15. *x* and *y* detector profiles obtained for the MCPPSD (*upper panels)* and the β telescope (*lower panels*). The profiles obtained with the simulations for pure axial coupling and for pure tensor coupling are superimposed.

To determine the plastic scintillator response function and reproduce the experimental energy spectrum (section 3.2.2), a value of $a_{\beta\nu}$ was also provided for each tested case (calibration curve and resolution). The $a_{\beta\nu}$ values have then been weighted with a factor $1/\chi^2$, where χ^2 is the associated chi-square resulting from the comparison between the experimental energy spectrum and the simulated one. Using this weighting method, the RMS of the $a_{\beta\nu}$ distribution was found to be $\sigma_{a_{\beta\nu}} = 8.0\times10^{-4}$. To test the sensitivity of the result to the choice of the weighting factor, the same calculation has been performed using a factor $1/\chi$, yielding $\sigma_{a_{\beta\nu}} = 8.4\times10^{-4}$. We kept this larger value as the uncertainty due to the plastic scintillator calibration. For the energy deposited E_{si} in the DSSSD we set a conservative 10% uncertainty on the results given by the GEANT4 simulations that were used in the calibration.

The uncertainties due to "accidentals" and "out-trap" background subtractions are only statistical. They are limited by the statistics of experimental background events which serve as normalization for the MC results. The uncertainty due to the "scattered" events was estimated by considering a 10% relative error on the β scattering yield provided by the GEANT4 simulations. This 10% relative error is based on the work of Hoedl [38], which compares a compilation of published electron scattering experimental data to several MC codes. To estimate the uncertainty due to the shake off ionization probability, we considered two extreme cases: a probability equal to zero, and a probability of 0.05, which corresponds to the double of the estimate by Patyk [29]. Preliminary results, obtained later in a dedicated measurement, confirmed that this uncertainty on the shake off probability is very conservative. The uncertainty on the trap RF voltage V_{RF} was estimated from the characteristics of the probe and the oscilloscope used to record the RF during the experiment. Combining all systematic errors quadratically, the final result is

$$a_{\beta\nu} = -0.3335(73)(75) \qquad (14)$$

where the first uncertainty is statistical and the second systematic.

Table 1. Dominant sources of systematic error, systematic uncertainties, and impact on the error of $a_{\beta\nu}$. The last column indicates the method used to estimate the parameters.

Source	Uncertainty	$\Delta a_{\beta\nu}$ (x 10^{-3})	Method
Cloud temperature	6.5%	6.8	off-line measurement
$\theta x_{\mathrm{MCPPSD}}$	0.003 rad	0.1	present data
$\theta y_{\mathrm{MCPPSD}}$	0.003 rad	0.1	present data
MCPPSD offset (x,y)	0.145 mm	0.3	present data
MCPPSD calibration	0.5 %	1.3	present data
d_{DSSSD}	0.2 mm	0.3	present data
E_{scint}	see text	0.8	present data
E_{si}	10%	0.8	GEANT4
"accidentals" and "out trap"	see text	0.9	present data
β Scattering	10%	1.9	GEANT4
Shake off	0 - 0.05	0.6	theoretical calculation
V_{RF}	2.5%	1.7	off-line measurement
total		7.5	

Figure 16 shows the final result compared with previous measurements of the β–ν angular correlation coefficient in pure Gamow-Teller transitions. The values from Carlson and from Allen *et al.* were obtained in ^{23}Ne decay, the others in ^{6}He decay. The present result is the most accurate among the experiment performed using the detection of the recoil ions and β particles in coincidence. The measurement presented here, performed with a different and independent method, confirms the result of Johnson *et al*. It is to be recalled that the reduced chi-square $\chi^2/\nu = 0.92$ for 105 degrees of freedom obtained in the present work corresponds to a P-value of 0.71. This is to be compared to a P-value of 0.055 for the Johnson *et al*. experiment, with a reduced chi-square $\chi^2/\nu = 1.69$ for 13 degrees of freedom [13]. The techniques used in the two experiments differ in a number of other aspects. First, the use of trapping techniques and the detection in coincidence of two decay products resulted in a larger signal to background ratio, by more than a factor of two compared to the Johnson *et al*. experiment. Furthermore, the measurement in an event by event mode of additional parameters (particle positions, energy of the β particle, RF phase, and time within the trapping cycle) allows a better control of possible systematic effects. With the efficiencies achieved for beam preparation and trapping and for the detection of coincidence events, the average counting rates in the present experiment was about 1 coincidence per second and about 100 single triggers per second. This is respectively three and one orders of magnitude lower than in the Johnson *et al*. experiment so that possible rate related systematic effects are expected here to have a smaller impact. The dominant contribution to the uncertainty in the Johnson *et al*. experiment was due to random variations of recoil energy spectra acquired sequentially, while in the present work, the precision limitation is mainly statistics. Both techniques are thus complementary.

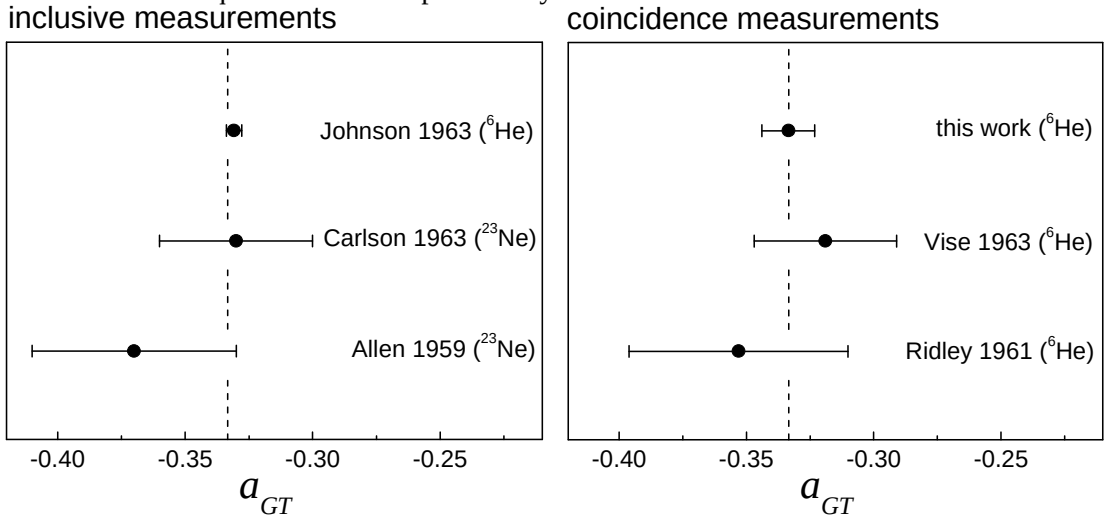

Figure 16. From top to bottom: $a_{\beta\nu}$ experimental values in pure Gamow-Teller transitions from [9], [12], [2] (left panel), present work, [10], and [11] (right panel).

The error bars show the quadratic sums of statistical and systematic uncertainties. The dashed lines indicate the value predicted by the SM.

5. Summary and conclusion

We have presented here the complete analysis of data taken in 2006 for the measurement of the β–ν angular correlation coefficient in the $^{6}He^{+}$ decay. This analysis required the implementation of detailed MC simulations as well as the control of the ion cloud temperature with additional off-line measurements.

The use of a transparent Paul trap for the confinement of the decaying radioactive ions offers a clean environment for such a measurement. By recording the positions and energies of both particles along with parameters of the setup, such as the RF phase, the main sources of systematic effects have been controlled to a high level of confidence. The present measurement is the most precise among the experiments performed in pure Gamow-Teller transitions by using the detection of the recoil ions and β particles in coincidence.

The result of the analysis was found to be consistent with the SM predictions. The precision is limited by statistics, and by the uncertainty on the ion cloud temperature. The efficiency of the LPCTrap apparatus has since been increased by a factor of about 20 [22] and new runs have been carried out. The results of these runs confirmed in particular that the issue related to the ion cloud is well under control [37]. The conclusion is that the main sources of systematic effects, namely the ion cloud temperature and the position of the recoil ion detector, can be inferred from the data so that their precision depends on the available statistics.

Several new generation radioactive ion beam facilities such as Spiral2 and FRIB, with higher production rates, will be operating in the coming ten years. A significant improvement of the statistics can thus reasonably be expected in future experiments. In this context, the use of a Paul trap for correlation measurements provides an alternative confinement technique to MOTs, with the potential to be applied to any atomic species.

Acknowledgments

We warmly thank former students and post-doc G. Darius, P. Delahaye and M. Herbane for their contribution at an earlier stage of the LPCTrap design and development. We would also like to express our gratitude to J. Bregeault, J.F. Cam, Ph. Desrues, B. Jacquot, Y. Merrer, H. Plard, Ph. Vallerand, and Ch. Vandamme for their constant assistance during the different phases of the project. We thank the GANIL staff for the preparation of an excellent ion beam. This work was supported in part by the Région Basse-Normandie.

References

[1] Feynman R P and Gell-Mann M 1958 *Phys. Rev.* **109** 193
[2] Allen J S, Burman R L, Herrmannsfeldt W B, Stähelin P and Braid T H 1959 *Phys. Rev.* **116** 134
[3] Severijns N, Beck M and Naviliat-Cuncic O 2006 *Rev. Mod. Phys* **78** 991
[4] Jackson J D, Treiman S B and Wyld H W Jr. 1957 *Phys. Rev.* **106** 517; 1957 *Nucl. Phys.* **4** 206
[5] Egorov V *et al.* 1997 *Nucl. Phys. A* **621** 745
[6] Adelberger E G, Ortiz C, García A, Swanson H E, Beck M, Tengblad O, Borge M J G, Martel I, Bichsel H and ISOLDE Collaboration 1999 *Phys. Rev. Lett.* **83** 1299
[7] Gorelov A *et al.*, 2005 *Phys. Rev. Lett.* **94** 142501
[8] Vetter P A, Abo-Shaeer J R, Freedman S J and Maruyama R 2008 *Phys. Rev. C* **77** 35502
[9] Johnson C H, Pleasonton F and Carlson T A 1963 *Phys. Rev.* **132** 1149
[10] Vise J B and Rustad B M 1963 *Phys. Rev.* **132** 2573.
[11] Ridley B W 1961 *Nuclear Physics* **25** 483
[12] Carlson T A 1963 *Phys. Rev.* **132** 2239
[13] Glück F 1998 *Phys. Lett. B* **436** 25
[14] Wang L B *et al.* 2004 *Phys. Rev. Lett.* **93** 142501
[15] Mueller P *et al* 2007 *Phys. Rev. Lett.* **99** 252501
[16] Brown L S and Gabrielse G 1986 *Rev. Mod. Phys.* **58** 233 and references therein
[17] Paul W 1990 *Rev. Mod. Phys.* **62** 531 and references therein

[18] Beck M *et al.* 2003 *Nucl. Instrum. Methods Phys. Res. A* **503** 567
[19] Kozlov V Yu *et al.* 2008 *Nucl. Instrum. Methods Phys. Res. B* **266** 4515
[20] Rodríguez D *et al.* 2006 *Nucl. Instrum. Methods Phys. Res. A* **565** 876
[21] Fléchard X *et al.* 2008 *Phys. Rev. Lett.* **101** 212504
[22] Duval F *et al.* 2008 *Nucl. Instrum. Methods Phys. Res. B* **266** 4537
[23] Darius G *et al.* 2004 *Rev. Sci. Instrum.* **75** 4804
[24] Liénard E *et al.* 2005 *Nucl. Instrum. Methods Phys. Res. Sect. A* **551** 375
[25] Glück F 1997 *Comput. Phys. Commun.* **101** 223
[26] Sirlin A 1967 *Phys. Rev.* **164** 1767
[27] Holstein B R and Treiman S B 1971 *Phys. Rev. C* **3** 1921
[28] Holstein B R 1974 *Rev. Mod. Phys.* **46** 789
[29] Patyk Z private communication
[30] Wauters L and Vaeck N 1996 *Phys. Rev. C* **53** 497
[31] Fléchard X *et al.* Temperature measurement of $^{6}He^{+}$ ions confined in a Paul trap, in Proc. of the TCP2010 International Conference, accepted for publication in *Hyp. Int.*
[32] http://simion.com/info/SIMION_8.html
[33] Ban G *et al.* 2004 *Nucl. Instrum. Methods Phys. Res. A* **518** 712
[34] http://geant4.cern.ch/
[35] Velten Ph *et al.* 2010 *AIP Conf. Proc.* **1224** 206
[36] Firestone R B 1999 *Table of Isotopes* 8th edition, Shirley V S (Berkeley: John Wiley & sons)
[37] Velten Ph *et al.* The LPCTrap experiment: measurement of the beta-neutrino angular correlation in $^{6}He^{+}$ decay using a transparent Paul trap, in Proc. of the TCP2010 Int. Conf., accepted for publication in *Hyp. Int.*
[38] Hoedl S A 2003 Novel Proton Detectors, Ultra-Cold Neutron Decay and Electron Backscatter, PhD Thesis, Princeton University